Dictyostelium myosin-IE is a fast molecular motor involved in phagocytosis

Ulrike Dürrwang[1], Setsuko Fujita-Becker[1], Muriel Erent[1], F. Jon Kull[2], Georgios Tsiavaliaris[3], Michael A. Geeves[4] and Dietmar J. Manstein[1,3,*]

[1]Abteilung Biophysik, Max-Planck Institut für medizinische Forschung, Jahnstr. 29, 69120 Heidelberg, Germany
[2]Dartmouth College, Department of Chemistry, 6128 Burke Laboratory, Hanover, NH 03755, USA
[3]Institut für Biophysikalische Chemie, OE 4350, Medizinische Hochschule Hannover, Carl-Neuberg-Str. 1, 30623 Hannover, Germany
[4]Department of Biosciences, University of Kent, Canterbury CT2 7NJ, UK
*Author for correspondence (e-mail: manstein@bpc.mh-hannover.de)

Accepted 19 October 2005
Journal of Cell Science 119, 550-558 Published by The Company of Biologists 2006
doi:10.1242/jcs.02774

Summary

Class I myosins are single-headed motor proteins, implicated in various motile processes including organelle translocation, ion-channel gating, and cytoskeleton reorganization. Here we describe the cellular localization of myosin-IE and its role in the phagocytic uptake of solid particles and cells. A complete analysis of the kinetic and motor properties of *Dictyostelium discoideum* myosin-IE was achieved by the use of motor domain constructs with artificial lever arms. Class I myosins belonging to subclass IC like myosin-IE are thought to be tuned for tension maintenance or stress sensing. In contrast to this prediction, our results show myosin-IE to be a fast motor. Myosin-IE motor activity is regulated by myosin heavy chain phosphorylation, which increases the coupling efficiency between the actin and nucleotide binding sites tenfold and the motile activity more than fivefold. Changes in the level of free Mg^{2+} ions, which are within the physiological range, are shown to modulate the motor activity of myosin-IE by inhibiting the release of adenosine diphosphate.

Supplementary material available online at
http://jcs.biologists.org/cgi/content/full/119/3/550/DC1

Key words: *Dictyostelium discoideum*, Phagocytosis, Phosphorylation, TEDS, Mg^{2+} concentration

Introduction

Myosins form a large family of mechano-enzymes that contain a common domain by which they bind to actin and convert the energy from the hydrolysis of ATP into movement along actin filaments. On the basis of sequence comparisons of their highly conserved catalytic domain, members of the myosin family have been grouped into 18 classes (Berg et al., 2001). Among the most prevalent and most widely expressed myosins are the monomeric, non-filamentous class I myosins. The conserved N-terminal motor domain of class I myosins, which contains the ATP- and actin-binding sites, is followed by one to six light-chain-binding IQ-motifs and more diverse C-terminal tail regions. More exact phylogenetic analysis shows that the class I myosins can be divided into at least four subclasses, designated Iα, Iβ, IC and Iγ (Gillespie et al., 2001). Here, we describe the functional properties of *Dictyostelium discoideum* myosin-IE, a member of the short-tailed myosin-Iα subfamily. Previously, we have solved the crystal structure of the myosin-IE motor domain and described the basic kinetic properties of a motor domain construct (Kollmar et al., 2002).

The regulation of class I myosins from *Acanthamoeba castellanii*, *Aspergillus nidulans* and *D. discoideum* is mediated by the phosphorylation of the TEDS rule phosphorylation site in the motor domain (Brzeska and Korn, 1996; Yamashita and May, 1998). Phosphorylation by a member of the p21-activated kinase (PAK) family occurs at a serine or threonine residue that is located 16 residues upstream of the highly conserved DALAK sequence (Bement and Mooseker, 1995). TEDS site phosphorylation is required for efficient actin activation of steady-state ATPase activity and actin-filament-based movement (Albanesi et al., 1983; Brzeska et al., 1989; Brzeska et al., 1999; Hammer et al., 1983; Ostap et al., 2002). In the case of *D. discoideum*, activation of ATPase activity by phosphorylation was shown for the subclass IC members myosin IB and myosin ID (Lee and Cote, 1995; Lee et al., 1996). The level of myosin IB phosphorylation was shown to increase threefold within a minute of stimulation of starving *D. discoideum* cells with the chemo-attractant cAMP, concomitant with the extension of pseudopodia (Gliksman et al., 2001). The importance of TEDS site phosphorylation for in vivo function was further demonstrated by the complementation of mutant cells lacking two class I myosins and displaying strong defects in growth, endocytosis and F-actin organization. Expression of the full-length myosin IB heavy chain rescued these defects, whereas expression of the S322A mutant failed to complement the null phenotype (Novak and Titus, 1998).

Here, we generated three types of recombinant constructs to analyze the functional properties of the *D. discoideum* myosin-Iα subfamily member myosin-IE. Cells expressing full-length myosin-IE fused to Yellow Fluorescent Protein (YFP) were used for cellular localization studies. YFP-tagged full-length constructs are referred to as YFP-myosin-IE or myosin-IE-YFP for the N- and C-terminally tagged version,

respectively. Motor domain constructs truncated at residue 698 (E698) were used to determine steady-state and transient kinetic parameters. To generate sufficient quantities of the protein for detailed analysis of motor activity and regulation in vitro, the myosin-IE motor domain was fused to an artificial lever arm consisting of two α-actinin repeats (E698-2R). To study the direct consequences of TEDS-site phosphorylation for the motor properties of myosin-IE, we performed in vitro motility assays with phosphorylated and dephosphorylated constructs. Additionally, we generated mutant versions of the motor domain and 2R-constructs, which allowed us to dissect both their kinetic and motor properties. The serine at the TEDS-site of these constructs was replaced by either an alanine residue, to mimic the unphosphorylated state, or a glutamate residue, to mimic the phosphorylated state. These constructs are referred to as S336A or S336E mutants in the following text.

Results

Cellular localization of myosin-IE

Myosin-IE is produced by *Dictyostelium* cells during vegetative growth and early development (Urrutia et al., 1993). In good agreement with these earlier results, we observed the highest levels of myosin-IE production 2 to 4 hours after removal of nutrients and no protein production during the late stages of development. The steady-state level of the *myoE* transcript falls gradually after 5 hours and the transcript cannot be detected after 14 hours of starvation-induced development (data not shown). The cellular localization of myosin-IE during early development was analyzed using cells producing full-length myosin-IE tagged either at the N- or C-terminus with YFP. Confocal fluorescence microscopy with fixed cells and analysis of living cells by epifluorescence showed that the position of the YFP tag did not effect the localization of the myosins. Myosin-IE is concentrated at the plasma membrane in crown-like structures and at the leading edge of the cell during cell movement. Immunofluorescence analysis confirmed the colocalization of YFP-myosin-IE and actin-rich structures (Fig. 1). The observed enrichment at crown-like structures resembles that observed with the actin-binding protein coronin, which participates in the remodelling of the cortical actin cytoskeleton that is responsible for phagocytosis and macropinocytosis (Bretschneider et al., 2002; de Hostos et al., 1991; Fukui et al., 1999). However, closer analysis shows that the proteins do not colocalize and are associated with different regions of crown-like structures (Fig. 1C).

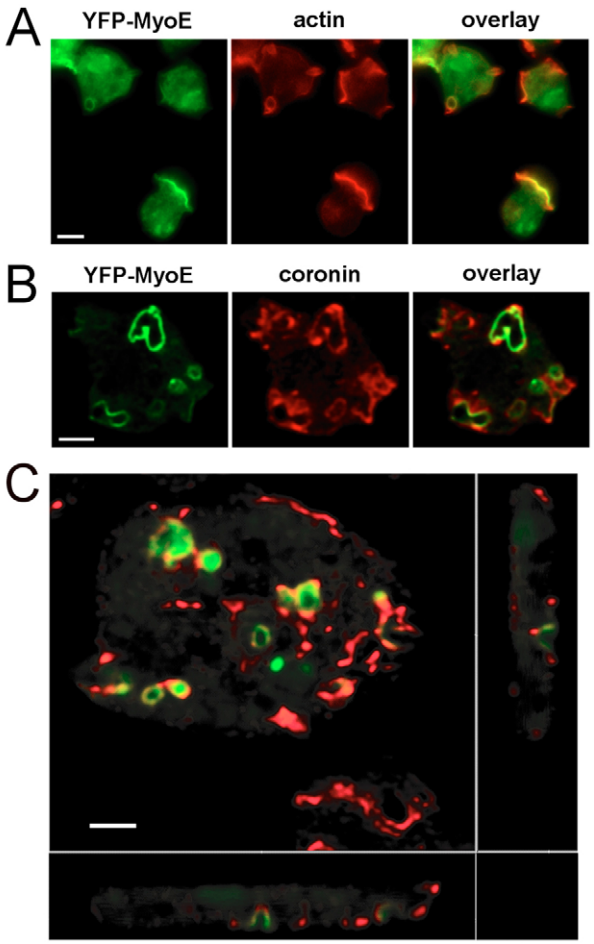

Fig. 1. Cellular localization of YFP-tagged myosin-IE. (A) Myosin-IE is preferentially localized at dynamic actin structures. Colocalization of YFP-Myosin-IE with actin demonstrated by epifluorescence microscopy. Actin was stained with TRITC-Phalloidin. YFP-Myosin-IE is shown in green, actin in red. (B) Localization of YFP-Myosin-IE (green) and coronin (red) at crown like structures as visualized by confocal microscopy. (C) Confocal analysis of the 3D distribution of YFP-Myosin-IE (green) and coronin. The *X-Z* and *Y-Z* views show myosin-IE predominantly at the side walls of large invaginations of the plasma membrane. Coronin localizes to the bottom of the invaginations and their upper rim. Bars, 10 μm (A,B); 3 μm (C).

Phagocytosis and fluid-phase endocytosis

Phagocytosis is an inducible actin-dependent process that is initiated by adhesion of a particle to any region on the surface of a *D. discoideum* cell. The dynamic redistribution of Imyosin-IE during phagocytosis could be visualized particularly well when the cells were starved to initiate multicellular development. Under these conditions some *D. discoideum* amoebas started to show cannibalistic behaviour. They were able to phagocytose other amoebas by nibbling pieces of these cells before ingesting them completely. The image sequence shown in Fig. 2A (see also Movie 1 in supplementary material) shows that myosin-IE decorates the entire phagocytic cup and the early phagosome during this process. After complete internalization, myosin-IE is shed from the phagosome with a similar timing as observed for actin and coronin (Maniak, 2001). Similarly, myosin-IE is associated with phagocytic cups and early but not late phagosomes during the uptake of yeast cells, which serve *D. discoideum* amoebas as a food source (Fig. 2B). Investigation of the time-dependent uptake of TRITC-labelled yeast revealed a 40% increase in the phagocytic activity of cells overproducing YFP-myosin IE in comparison to the wild type (Fig. 3A). The increase was observed for the initial rate of uptake and the steady-state level that was reached after approximately 35 minutes. In contrast to this marked increase in phagocytic activity of the myosin-IE overproducing cells, they showed a 30% reduction in the initial rate of the fluid phase marker Fluorescein-labelled dextran (Fig. 3B).

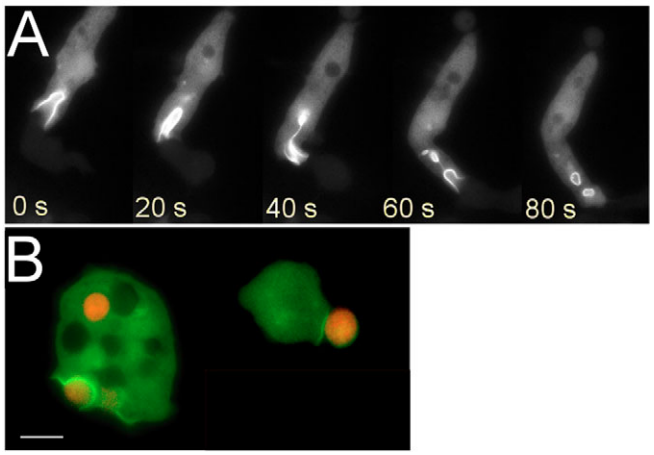

Fig. 2. Localization of myosin-IE during phagocytosis. (A) Myosin-IE was observed to be associated with the phagocytic cup during the process of ingesting bits of other cells, and the early phagosome (see Movie 1 in supplementary material). (B) Phagocytosis of yeast cells (red) by *D. discoideum* amoeba. Myosin-IE associates with the phagocytic cup shortly after particle docking. It remains associated with the phagocytic cup during engulfment and dissociates from the phagosome within 2 minutes of completion of uptake. Bar, 3 μm.

Actin-activation of myosin-IE is dependent on TEDS-site phosphorylation

Motor domain constructs E698 and E698(S336E) were used to measure steady-state ATPase activity. E698(S336A) displayed very low actin affinity and could not be purified in sufficient quantities for detailed kinetic analysis. In the absence of actin filaments, wild-type and S336E mutant constructs displayed similar ATPase activity. To determine the maximum values of the ATPase activity and the efficiency of coupling between actin and nucleotide binding, we measured the ATPase rates with actin concentrations in the range of 0 to 60 μM F-actin. The value for k_{cat}/K_{app} is well defined by the initial slope of the data fitted to the Michaelis-Menten equation. However, the individual values k_{cat} and K_{app} can only be estimated, as the maximum F-actin concentration that could be used for our measurements is lower than K_{app}. The ATPase activity of the S336E mutant was 30-fold activated by 20 μM F-actin and showed a hyperbolic dependency on actin concentration. The coupling efficiency of the S336E mutant of E698 was ten times greater than that of the partially phosphorylated wild-type construct, which displayed only a ninefold activation in the presence of 20 μM F-actin. After treatment with λ-phosphatase, no actin activation was observed within the margin of error for the ATPase activity of the wild-type construct and coupling efficiency was at least 100-fold reduced compared with the S336E mutant.

TEDS-site phosphorylation of myosin-IE stabilizes the actomyosin complex

The rate of actin binding was measured following the exponential decrease in pyrene fluorescence, observed on binding of an excess of pyrene-actin to the myosin-I construct. The observed rate constants were plotted against pyrene-actin concentration, and k_{obs} values were linearly dependent upon actin concentration over the range from 0.5 to 3 μM actin (data not shown). The second-order rate constants of pyrene-actin binding ($\mathbf{k_{+A}}$) were obtained from the slope of the plot and the resulting values are summarized in Table 1. The $\mathbf{k_{+A}}$ values were unaffected by the S336E mutation.

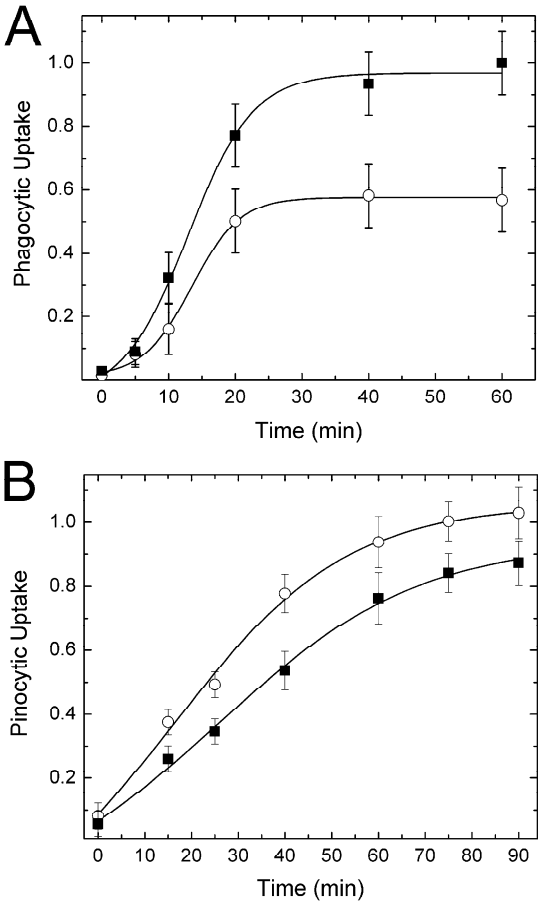

Fig. 3. The role of myosin-IE in phagocytosis and pinocytosis. (A) Phagocytotic ability was assayed by following the uptake kinetics of TRITC-labelled yeast cells in *D. discoideum* overproducing YFP-myosin-IE (■) and wild-type cells (○). (B) Uptake kinetics of the fluid-phase marker FITC-dextran in *D. discoideum* overproducing YFP-myosin-IE (■) and wild-type cells (○).

The rate constant for actin dissociation ($\mathbf{k_{-A}}$) was determined by chasing pyrene actin with a 40-fold excess of unlabeled actin. The observed process could be fitted to a single exponential, where k_{obs} corresponds directly to $\mathbf{k_{-A}}$ (data not shown). The complex of the S336E mutant and actin dissociates four times more slowly than that of the partially phosphorylated wild-type protein construct and actin. The dissociation equilibrium constant ($\mathbf{K_A}$) for actin binding is calculated from the ratio of $\mathbf{k_{-A}}$ and $\mathbf{k_{+A}}$. The slower dissociation rate of the actomyosin complex results in a higher actin affinity for the S336E mutants. Treatment of the myosin constructs with apyrase, to remove any residual ADP, did not result in significant changes in the observed rate constants.

Binding of nucleotide to the myosin-IE motor domain

The rate constants measured for nucleotides binding to the wild-type construct and the TEDS-site mutants were identical. Therefore, we will refer only to the wild-type construct

Table 1. Interaction of myosin-IE with filamentous actin

	Michaelis-Menten parameters				Actin affinity		
Myosin construct	Basal (second^{-1})	k_{cat} (second^{-1})	K_{app} (μM)	k_{cat}/K_{app} (μM^{-1}second^{-1})	$\mathbf{k_{+A}}$ (μM^{-1}second^{-1})	$\mathbf{k_{-A}}$ (msecond^{-1})	$\mathbf{K_A}$ (nM)
E698*	0.04±0.01	2.2±0.2	118±20	0.017	2.6±0.1	5.5±0.1	2.1
E698(S336E)	0.08±0.01	15.4±3.0	91±30	0.170	2.9±0.2	1.5±0.1	0.5
M765	0.08±0.01	2.6±0.4	73±20	0.036	0.8±0.1	2.2±0.2	2.9

Results for ATPase activity measurements are given as P_i liberated/myosin head/s. Uncertainties represent standard deviations of the mean values. Reactions were performed as described in the Materials and Methods. *Partially phosphorylated protein as purified from *D. discoideum* amoeba.

although all measurements were performed with the wild-type and mutant constructs. In the case of the S336A mutant, we used E698-2R instead of the motor domain construct for these measurements. We have previously shown that the attachment of an artificial lever arm does not affect the actin and nucleotide binding kinetics of myosin constructs (Ito et al., 2003; Kollmar et al., 2002; Kurzawa et al., 1997; Ruff et al., 2001). The results of the kinetic measurements with E698 and E698-2R confirmed this result (data not shown).

Structural studies have shown that myosin-IE has the conserved tryptophan at the tip of the relay loop (Trp433) that reports conformational changes associated with ATP hydrolysis (Batra and Manstein, 1999; Kollmar et al., 2002). In addition, three more tryptophan residues are located in the motor domain at positions 267, 363, and 645. Therefore, rates of ATP binding (K_1k_{+2}) and ADP binding (k_{-6}/K_7) could be determined from the increase in intrinsic protein fluorescence following the addition of excess ATP or ADP. The increase in fluorescence upon binding to myosin-IE was 9% for ATP and 6% for ADP binding. At high ATP concentrations, the rate of binding saturates for myosin-IE at 900 second^{-1}. For most myosins this maximum rate constant has been attributed to the rate constant for the ATP hydrolysis step (k_{+3}+k_{-3}), which is signalled by the fluorescence change of the relay-loop tryptophan (Batra and Manstein, 1999). The values obtained with the myosin-IE constructs are very high compared with most myosins and are comparable with those measured for myosin-V (De La Cruz et al., 1999). ATP binding produced a larger fluorescence increase than the binding of ADP. Therefore, the displacement of ADP by ATP could be followed from the net increase in fluorescence upon displacement of excess ADP from the myosin-ADP complex by the addition of a larger excess ATP. The rate of ADP release from E698 was 3.1 second^{-1}.

Binding of the nucleotide analogues mantATP and mantADP was measured by following fluorescence enhancement after mixing with the myosin constructs. The results of these measurements were analyzed as described previously (Batra et al., 1999) and are summarized in Table 2. They show that the apparent second-order association rate constants (K_1k_{+2} or k_{-6}/K_7) are similar for ATP, ADP and the mant analogues.

At intermediate ADP concentrations (<40 μM) the reaction observed upon adding excess ATP could be described by two exponentials. The amplitude of the fast phase was smaller and that of the slow phase larger with increasing ADP. The fast process is the rate at which ATP binds to unliganded myosin (K_1k_{+2}[ATP]) and the slow process is the rate at which ATP replaces ADP bound to myosin (k_{+6}). Accordingly the slow phase was independent of the concentration of ATP used. The dependence of the amplitude on the ADP concentration was described by a hyperbolic function, which defines the equilibrium constant of ADP binding to the myosin-IE (K_6K_7). The value obtained for E698 was 7.1 μM (Table 2).

Table 2. Rate and equilibrium constants of the actomyosin-I ATPase cycle

Nucleotide	Rate constant	D692*	E698†	M765
Nucleotide binding to M				
ATP	K_1k_2 (μM^{-1}second^{-1})	0.66±0.01	0.96±0.03	0.56±0.03
	k_{max} (second^{-1})	640±10	900±30	30±1
mantATP	K_1k_2 (μM^{-1}second^{-1})	0.53±0.02	0.91±0.01	0.81±0.02
ADP	k_{-6}/K_7 (μM^{-1}second^{-1})	0.98±0.02	0.34±0.02	n.a.
	k_{+6} (second^{-1})	0.60±0.002	3.13±0.03	n.a.
	K_D (μM)‡	1.9±0.3 (0.6)	7.1±0.4 (9.2)	14§
mantADP	k_{-6}/K_7 (μM^{-1}second^{-1})	0.87±0.01	0.79±0.01	0.36±0.004
Nucleotide binding to A·M				
ATP	$\mathbf{K_1k_{+2}}$ (μM^{-1}second^{-1})	0.49±0.01	0.40±0.002	0.16±0.002
	$\mathbf{k_{+2}}$ (second^{-1})	960±20	750±20	490±20
ADP	$\mathbf{k_{-AD}}$ (second^{-1})	n.d.	30	>100
	$\mathbf{K_{AD}}$ (μM)	75±4¶	12±2¶	253±11
	$\mathbf{K_{AD}}/K_D$	40	2	18

*Myosin-ID motor domain (Fujita-Becker et al., 2005); †Identical values were obtained with the wild-type, S-to-A and S-to-E constructs; ‡Values are derived from biphasic ADP dissociation reactions at different ADP concentrations. Values in brackets are obtained from the calculated $k_{+6}/(k_{-6}/K_7)$; §Batra et al., 1999; ¶Value refers to the S-to-E mutants of the myosin-I motor domain constructs. The $\mathbf{K_{AD}}$ value for D692(S-to-A) is 118 μM. Uncertainties represent standard deviations of the mean values. n.a., not applicable; n.d., not determined. Experimental conditions: 20 mM MOPS, pH 7.0, 5 mM $MgCl_2$, 100 mM KCl, 20°C.

ATP-induced dissociation of actomyosin

The binding of ATP to the acto·myosin-IE complex could be followed by observing the increase in fluorescence of pyrene-actin as the complex dissociates following addition of excess ATP. The observed transients had two components that could be described by two exponential functions. The observed rate constant of the fast phase is linearly dependent upon ATP concentration in the range of 5 to 25 μM (Fig. 4A). The apparent second-order binding constant $\mathbf{K_1k_{+2}}$ is defined by the gradient of the plot. Values of 0.40 $\mu M^{-1}second^{-1}$ were obtained for the wild type and S336E construct. At high ATP concentrations (>2 mM) the observed rate constants saturate, and the dependence on the ATP concentration could be described by a hyperbola, where the maximum value of k_{obs} was 750 $second^{-1}$ and this defines the value of $\mathbf{k_{+2}}$ (Fig. 4B).

The slow phase, which is apparent at ATP concentrations greater than 200 μM, has a k_{obs} of ~30 $second^{-1}$ and corresponds to approximately 20% of the total amplitude. The k_{obs} is of the same order as the rate constant for ADP release from acto·E698. However, extensive treatment with apyrase did not remove the slow phase. It is therefore not due to contaminant ADP.

Competitive binding of ATP and ADP to acto·myosin-IE

The affinity of ADP for the actomyosin complex ($\mathbf{K_{AD}}$) was determined from the inhibition of the ATP-induced dissociation of actomyosin by ADP. The presence of small amounts of ADP in the complex of actin and E698(S336E) enhanced the slow phase of the observed biphasic dissociation reaction (Fig. 4C). Over the concentration range 0 to 80 μM ADP, the k_{obs} values for the two phases were independent of the ADP concentration. The observed rate constant of the fast phase was identical to that of the major phase without ADP. The rate constant for the slow phase was identical to the rate constant of ADP dissociation from the actomyosin complex (30 $second^{-1}$). The amplitude of the fast phase decreased and the amplitude of the slow phase increased as the ADP concentration was increased (Fig. 4D). The total amplitude remained constant, compatible with little dissociation of actin by ADP. The amplitude dependence could be described by hyperbolic functions with a $\mathbf{K_{AD}}$ of 12 μM for E698(S336E).

TEDS-site phosphorylation increases the motile activity of myosin-I constructs

Motor function was directly analyzed by measuring the gliding velocity of actin filaments on surfaces decorated with E698-2R in an in vitro motility assay (Kron and Spudich, 1986). To investigate regulation by TEDS-site phosphorylation, we treated the motor domain construct carrying an artificial lever arm with λ-phosphatase to generate the dephosphorylated form or with myosin-I kinase (MIHCK) (Brzeska et al., 1999) to generate the phosphorylated form. Additionally, we used constructs with artificial lever arms in which the serine at the TEDS site was mutated to either glutamate or alanine, to mimic the phosphorylated and dephosphorylated states of the protein. For each construct, the movement of at least 50 filaments was followed and the velocity determined. The average sliding

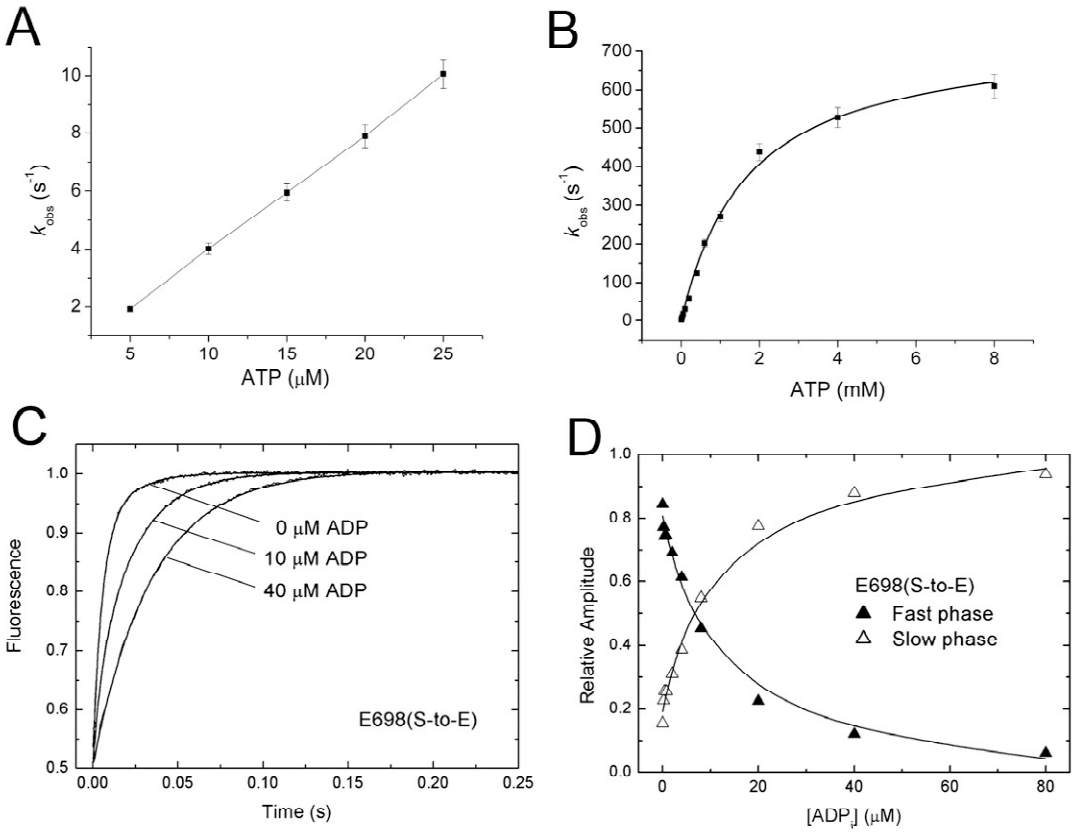

Fig. 4. Transient kinetic analysis of the interaction of Myosin-IE with actin and nucleotides. (A) ATP-induced dissociation of the actomyosin complex. The observed rate constants for E698 is linearly dependent on the ATP concentration in the range 5-25 μM. The apparent second-order rate constant for ATP binding to actomyosin ($\mathbf{K_1k_{+2}}$) was determined from the slope of the line. (B) The data over the range from 5 μM to 8 mM were fitted to a hyperbola. The rate constants for the isomerization step are given by the plateau values. (C) ADP inhibition of ATP-induced dissociation of the actomyosin complex of E698(S336E). Small amounts of ADP in the complex of E698(S336E) and pyrene-actin produced biphasic dissociation reactions. (D) Relative amplitudes of the two exponentials in dependency on the ADP concentration. The data are fitted with hyperbolae resulting in a $\mathbf{K_{AD}}$ of 12 μM for the slow phase (△) and the fast phase (▲).

Table 3. Sliding velocity of actin filaments

	M765-2R (μm/second)	E698-2R (μm/second)
Untreated*	0.82±0.07	0.18±0.05
Phosphatase treated*	n.a.	0.08±0.03
Kinase treated*	n.a.	0.42±0.04
(S336A)*	n.a.	no motility
(S336E)*	n.a.	0.35±0.06
High [ATP]†	0.83±0.08	0.87±0.15‡

*Experimental conditions: 2 mM ATP, 4 mM $MgCl_2$, 25 mM imidazole, pH 7.4, 25 mM KCl, 1 mM EGTA, 10 mM DTT, 30°C; †Experimental conditions: 10 mM ATP, 4 mM $MgCl_2$, 25 mM imidazole, pH 7.4, 25 mM KCl, 1 mM EGTA, 10 mM DTT, 30°C; ‡Measured for construct E698-2R (S336E). Uncertainties represent standard deviations of the mean values.

velocities are summarized in Table 3. The phosphorylated form of E698-2R moved actin filaments more than five times faster than the dephosphorylated form. Similar changes in motile activity were observed for the TEDS-site mutants. The S336E mutant of E698-2R moved actin with 0.35 μm/second, whereas the S336A mutant moved too slowly to allow accurate measurements.

The motile activity of myosin-IE is inhibited by free Mg^{2+}

The detailed analysis of the dependence of the motile activity of myosin-IE on ATP and Mg^{2+} concentrations revealed that myosin-IE can produce even faster movement than that observed under the standard assay conditions generally used for the in vitro motility assay (Kron and Spudich, 1986). As long as the Mg^{2+} concentration did not exceed the ATP concentration, a velocity of approximately 0.9 μm/second was observed for E698-2R(S336E). By contrast, *D. discoideum* myosin II motility was not affected by similar changes in Mg^{2+} and ATP concentrations. The observed changes in the motile activity of the myosin IE construct appear to be the result of ATP acting as chelator of Mg^{2+}. The equilibrium dissociation constants for Mg^{2+} binding to ATP is 87 μM (Michailova and McCulloch, 2001). Our results indicate that excess free Mg^{2+} ions cause a more than threefold reduction in the motile activity of E698-2R(S336E) with an apparent inhibition constant (K_i) of approximately 0.8 mM.

To elucidate how changes in the Mg^{2+} concentration affect the ATPase cycle, we examined the release of ADP from actomyosin. The rate of ADP release from acto·E698 can be measured by displacing the bound ADP with excess Mg^{2+}-ATP. In this case the apparent value of ADP release dropped from 56.2±2.6 $second^{-1}$ at 0 mM Mg^{2+} to 22.6±1.9 $second^{-1}$ at 20 mM Mg^{2+} with an apparent ADP affinity of 0.99±0.3 mM (Fig. 5). Therefore, our data indicate that elevated Mg^{2+}-concentrations can inhibit ADP release by about 2.5-fold for myosin-IE. The apparent K_i for ADP release from acto·E698 is similar to that derived from the motility data.

For completeness, we also examined the effect of free Mg^{2+} on the rate of ADP release from myosin-IE in the absence of actin. Myosin-IE displayed an apparent affinity for Mg^{2+} of 0.3 mM and higher Mg^{2+} concentrations led again to a 2.5-fold inhibition of the rate of ADP release.

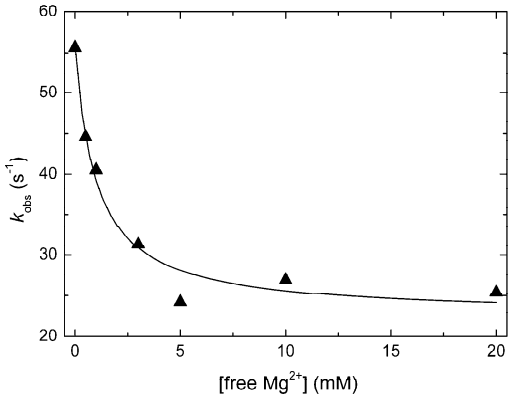

Fig. 5. Inhibition of Myosin-IE by free Mg^{2+}. The rate of ADP dissociation from Myosin-IE is dependent on the Mg^{2+} concentration. The k_{obs} for the displacement of 30 μM ADP from 0.25 μM E698 by 500 μM MgATP is plotted over the range 0 to 20 mM free-Mg^{2+} concentration. The data were fitted to a hyperbola and indicate a K_d of 0.99±0.3 mM.

Discussion

Previously, we have shown that the topology and core structural elements of the *D. discoideum* myosin-IE motor domain are very similar to those in myosin-II (Kollmar et al., 2002). Differences in the structure of surface loops appear to fine-tune the nucleotide- and actin-binding properties, whereas changes in the contact between the relay helix and the converter domain allow myosin-IE to rotate its lever through a larger angle and to produce a larger power stroke. Owing to its well-characterized structure and compact size, the myosin-IE motor domain was used as building block in the generation of an artificial backwards-moving myosin by protein engineering (Tsiavaliaris et al., 2004). Here, we focus on the functional properties of the protein, including cellular localization, interaction with actin, nucleotide binding, motor activity, and regulation of motor activity.

Myosin-IE is a fast class Iα myosin

Myosin-IE has an ADP coupling ratio ($\mathbf{K_{AD}}/K_D$) of 2 compared with 18 for *Dictyostelium* myosin II (Kurzawa et al., 1997). This is mostly the result of a ~20-fold increased affinity for ADP in the presence of F-actin ($\mathbf{K_{AD}}$). In addition, myosin-IE displays the biphasic dissociation of actomyosin first identified for Myr1 (Coluccio and Geeves, 1999; Geeves et al., 2000; Nyitrai and Geeves, 2004). The similar properties of myosin-IE, brush-border myosin-I (BBM-I) and Myr1 in regard to their interaction with ADP suggest that myosin-IE may share other features like the ADP-induced neck movement and the double step in the laser trap with these class Iα myosins (Jontes and Milligan, 1997; Jontes et al., 1995; Veigel et al., 1999). It has been proposed that these properties make ADP release very sensitive to the load on the head of class Iα myosins and are indicative of myosins designed to carry large loads or to crosslink load-bearing actin filaments (Coluccio and Geeves, 1999; El Mezgueldi et al., 2002). However, single-headed myosin-IE constructs move at a velocity similar to rabbit skeletal muscle myosin subfragment-1 (S1) and recombinant, S1-like *D. discoideum* myosin II constructs (Manstein et al., 1989; Ruff et al., 2001; Toyoshima et al., 1987). The velocity observed for the E698-2R construct is thus too fast to be consistent with a crosslinking function. The Mg^{2+}-dependent modulation of myosin motor activity that was recently described for myosin-ID and mammalian myosin V may,

at least in part, explain these apparently contradictory observations (Fujita-Becker et al., 2005; Rosenfeld et al., 2005). Our results show that ADP-release from acto·myosin-IE is affected by changes in the concentration of free Mg^{2+} that are within the physiological range. The apparent K_i of ~800 μM for free Mg^{2+} makes the coordination of the Mg^{2+} ion at the nucleotide-binding site responsive to changes that lie well within the range of physiological free-Mg^{2+} concentrations in *D. discoideum* and many other cell types (Michailova and McCulloch, 2001; Satre and Martin, 1985). The resulting threefold modulation of myosin-IE motor velocity at zero load conditions is small but the concomitant increase in the ability of the protein to generate tension needs to be considered as well. Our results indicate that higher concentrations of free Mg^{2+} stabilise the tension-bearing A·M·ADP state and shift the system from the production of rapid movement towards the generation of tension. Motility, ATPase activities and ADP release were measured in this study under low or zero load conditions and experiments are now underway to test if myosin-IE shows any significant load dependence of these activities. Inhibition of ADP release by Mg^{2+} has not been observed for the extensively studied class II myosins, but it seems to be more common amongst unconventional myosins. Therefore, the fast motor activity of other members of the myosin family may have been concealed by the presence of high concentrations of free Mg^{2+} and changes within the physiological range of free Mg^{2+} concentrations need to be considered to play an important role in modulating the motor activity of unconventional myosins.

It is interesting to note that for myosin-IE the rate constant for ADP release ($\mathbf{k_{-AD}}$) is of the same order as k_{cat}. Therefore, although the conditions of the two measurements (k_{cat} and $\mathbf{k_{-AD}}$) are not identical, it is likely that the rate of ADP release contributes significantly to defining both k_{cat}, the maximal ATPase activity in the presence of F-actin, and V_{Max}, the maximal velocity in the in vitro motility assay. Moreover, the similarity of $\mathbf{k_{-AD}}$ and k_{cat} is indicative of a high duty ratio myosin with a long-lived A·M·ADP complex. The high apparent value of the hydrolysis step (k_{+3}+k_3) is consistent with this view. Additionally, it raises the question why this monomeric myosin displays kinetic properties normally associated with processive myosins. At this stage we can only speculate that they are an indication that myosin IE works in small coordinated groups.

The motile activity of myosin-IE is regulated by TEDS-site phosphorylation

The direct fusion of an artificial lever arm to the myosin-IE motor domain facilitates the cloning, expression and purification of single polypeptide constructs with similar motile activity to the native myosin (Ruff et al., 2001). The myosin-IE neck region, consisting of two IQ motifs and the associated light chains, has a length of approximately 9 nm compared with 12 nm for the artificial lever arm consisting of 2 α-actinin repeats. Therefore, the velocity observed for the E698-2R constructs may be 30% faster than the expected velocity of the native protein. The in vitro motility data show that freshly purified E698-2R is partially phosphorylated at the TEDS site and can be efficiently converted into the phosphorylated and dephosphorylated forms of the protein by the use of MIHCK and λ-phosphatase, respectively. A regulatory effect of TEDS-site phosphorylation on motor activity is supported by the more than fivefold faster movement of the phosphorylated form of E698-2R. Similar results were obtained with the TEDS site mutants S336A and S336E, although the motile activity of the S336A mutant was below the detection limit of our experimental set-up.

Steady-state kinetic measurements confirm that the presence of a negative charge at the TEDS-site increases the ability of actin to stimulate myosin-IE ATPase activity. Both the maximum turnover rate (k_{cat}) and the apparent second-order binding constant for F-actin (k_{cat}/K_{app}), which is a measure of the coupling efficiency between actin binding and ATP turnover, are increased. The results of our transient kinetics experiments show that charge changes at the TEDS site do not affect the interactions between the myosin motor and nucleotides, but the presence of a negative charge contributes to more than fourfold stabilization of the acto·myosin-IE complex. This is primarily due to a stabilization of bound F-actin via an estimated 20-fold reduction in the actin off-rate ($\mathbf{k_{-A}}$). Similar effects have been observed following the introduction of a single negative charge in the actin-binding region of myosin-II (Furch et al., 1998). Additionally, the results of the kinetic analysis of the myosin-IE motor domain constructs are in good agreement with effects of *A. castellanii* myosin-IC by heavy-chain phosphorylation (Ostap et al., 2002).

Cellular function of myosin-IE

Our results show that myosin-IE colocalizes with actin in actively extending regions of the cell, crown-like structures and the phagocytic apparatus. *D. discoideum* is an ideal system to study the function of motor proteins because the cells display many different types of cellular and intracellular motility and the availability of sophisticated molecular genetic tools. However, previous attempts to determine the function of individual class I myosins by depletion experiments in *D. discoideum* did not produce phenotypic changes that helped to clearly identify their cellular function and suggested functional redundancy of myosin-I isoforms (Jung et al., 1996; Novak et al., 1995; Titus et al., 1993). By contrast, overproduction of myosin-IB in *D. discoideum* produced clear phenotypic changes suggesting a role of the protein in the formation of cell surface extensions and cell migration (Novak and Titus, 1997). We decided to use the latter approach to study the cellular function of myosin-IE. Consistent with the results of the cellular localization studies, increased production of the YFP-tagged form of myosin-IE results in a faster rate of phagocytic uptake and an higher steady-state level with regard to the number of internalized particles per cell. The concomitant decrease in pinocytosis suggests that the role of myosin-IE in phagocytosis is rather specific.

In summary, our results allow a clear assignment of the cellular role of myosin-IE. They show that heavy chain phosphorylation at the TEDS site serves as a general on-off switch for the motor and explain how changes in the concentration of free Mg^{2+} can adjust myosin-IE motor activity to apparently opposing requirements with regard to fast movement and tension generation.

Materials and Methods

Materials

D. discoideum cells were grown as described previously (Manstein and Hunt, 1995). *D. discoideum* AX3-ORF$^+$ cells were transformed with the expression plasmids by electroporation (Egelhoff et al., 1991). Transformants were selected and grown in

the presence of 10 μg/ml G418 (Invitrogen). The Myosin-IE constructs were purified as described previously for myosin-II head fragments (Manstein and Hunt, 1995). Actin was prepared as described (Spudich and Watt, 1971) and labelled with pyrene (pyr-actin) as previously described (Coates et al., 1985). The 2′(3′)-*O*-(*N*-methylanthraniloyl) derivative of ATP (mantATP) was prepared by reaction with *N*-methylisatoic anhydride as described by Hiratsuka (Hiratsuka, 1983), except that after reaction it was purified on a DEAE-cellulose column as described in Woodward et al. (Woodward et al., 1991). The 2′(3′)-*O*-(*N*-methylanthraniloyl) derivative of ADP (mantADP) was prepared by incubation of mantATP with rabbit fast skeletal myosin subfragment-1 (S1) in a buffer containing 25 mM HEPES, 25 mM KCl and 4 mM $MgCl_2$, followed by gel filtration on a desalting column.

Plasmid construction and mutagenesis

Genomic DNA was isolated from *D. discoideum* strain AX2 according to (Bain and Tsang, 1991). PCR-directed mutagenesis was used to isolate a *myoE* gene fragment encoding the motor domain with a unique *Bam*HI site at the 5′ end of the coding region and a unique *Xho*I site at position 698. The PCR product was digested with *Bam*HI and *Xho*I and cloned into pDXA-3H (Manstein et al., 1995), which carries sequences for the fusion of a C-terminal His_8-tag. For the production of a motor domain construct fused to *D. discoideum* α-actinin repeats 1 and 2 (2R), the plasmid was digested with *Xho*I and *Sph*I. A DNA fragment encoding 2R, a $(Gly\text{-}Ser\text{-}Gly)_4$ linker, EYFP and a His_8 tag was obtained as *Xho*I/*Sph*I fragment from pM790-2R-EYFP (Knetsch et al., 2002) and inserted in the myosin-IE motor domain expression plasmid. To produce full-length myosin-IE fused to EYFP, *myoE* was amplified by PCR and unique *BamH*I and *Xho*I sites were created at the 5′ and 3′ end of the gene, respectively. Using *BamH*I and *Xho*I the PRC product was cloned in the vectors pDXA-MCS-EYFP or pDXA-EYFP-MCS (Knetsch et al., 2002) for the N- and C-terminal fusion with EYFP, respectively. TEDS-site mutants were generated by PCR-directed mutagenesis.

Direct functional assays

Actin-sliding motility was measured as described previously (Anson et al., 1996; Kron and Spudich, 1986). TEDS-site phosphorylation was performed by mixing 1 mg/ml E698-2R with 0.027 mg/ml activated kinase and incubation in the presence of 1 mM EGTA, 3 mM $MgCl_2$ and 2 mM ATP at 30°C for 20 minutes. MIHCK was activated by autophosphorylation at 30°C for 20 minutes in a buffer containing 100 mM imidazole, pH 7.0, 4 mM ATP, 6 mM $MgCl_2$ and 2 mM EGTA (Brzeska et al., 1999). *A. castellanii* myosin I heavy chain kinase (MIHCK) was generously provided by E. D. Korn and H. Brzeska (Laboratory of Cell Biology, National Heart, Lung and Blood Institute, Bethesda, MD). Dephosphorylation was performed by incubation of 1 mg/ml E698-2R with 4000 U/ml λ-protein phosphatase in the presence of 4 mM DTT, 2 mM $MnCl_2$ and 0.01% Brij 35 at 30°C for 30 minutes. Free Mg^{2+} concentrations were calculated using Maxchelator software (Epel, 2003). Phagocytosis and fluid-phase endocytosis were measured as described previously (Maniak et al., 1995; Wienke et al., 1999).

Kinetic measurements

Stopped-flow measurements were performed at 20°C with a Hi-tech Scientific SF-61 DX2 double-mixing stopped-flow system using procedures and kinetic models described previously (Batra et al., 1999; Cremo and Geeves, 1998; Furch et al., 1999; Kurzawa and Geeves, 1996). The binding and hydrolysis of ATP by *D. discoideum* myosin head fragments was analyzed in terms of the seven-step model (see Scheme 1 in Fig. 6) described by Bagshaw and co-workers (Bagshaw et al., 1974). Transients in the presence of actin were analyzed in terms of Schemes 2 and 3 (Fig. 6) (Millar and Geeves, 1983; Siemankowski and White, 1984).

Steady-state ATPase activities were measured at 25°C with the NADH-coupled assay (Furch et al., 1998) in a buffer containing 25 mM HEPES, 25 mM KCl, and 4 mM $MgCl_2$. The myosin concentration was 0.25-1 μM. NADH oxidation was followed using the change in absorption at 340 nm in a Beckman DU-650 spectrophotometer. Values for k_{cat} and K_{app} were calculated from fitting the data to the Michaelis-Menten equation. The apparent second-order rate constant for actin binding (k_{cat}/K_{app}) was obtained from the calculated ratio of both values. Alternatively the data at concentrations of actin much lower than K_{app}, could be fitted to a straight line and k_{cat}/K_{app} was determined from the slope of this line. Interpretation of transient kinetics data was done as described previously (Batra et al., 1999; Cremo and Geeves, 1998; Furch et al., 1998; Kurzawa et al., 1997).

Immunofluorescence

Cells were grown on coverslips overnight and fixed by immersion in methanol at –85°C, warmed up to –35°C and then plunged in PBS (137 mM NaCl, 2.7 mM KCl, 1.5 mM KH_2PO_4 and 8.1 mM Na_2HPO_4, pH 7.2) at room temperature. To block non-specific binding of antibodies, cells were incubated in 3% BSA in PBS (pH 7.4) followed by incubation with a monoclonal anti-coronin antibody mAb 176-2-5 (diluted 1:20 in blocking buffer) or with a monoclonal anti-α-tubulin antibody (diluted 1:500) (Sigma) for 1 hour at room temperature (RT). After extensive washing in PBS, coverslips were incubated with a Texas-Red-conjugated secondary antibody (Amersham Biosciences), diluted 1:500 in blocking buffer for 1 hour at RT. For staining of F-actin, cells were fixed with 1% paraformaldehyde, 0.1% glutaraldehyde, 0.1% Triton X-100 in PHEM (60 mM PIPES pH 6.4, 25 mM HEPES, 10 mM EGTA, 2 mM $MgCl_2$). Cells were treated twice with 2 mg/ml $NaBH_4$ in PHEM to reduce background fluorescence. After washing, cells were blocked in gel/BSA buffer (20 mM Tris-HCl pH 8.0, 0.9% NaCl, 0.1% BSA, 0.02% gelatine) and incubated for 1 hour with 150 nM TRITC-Phalloidin (Sigma) at RT. After extensive washing coverslips were mounted on slides using Prolong® Antifade kit (Molecular Probes).

Fluorescence microscopy was performed using an Olympus IX70 inverted microscope with a Zeiss Plan-Apochromat 100× objective (NA 1.4) and a Chroma FITC-Cy3 filter set. Images were recorded with an Imago CCD camera (TILL Photonics). Images of living cells were recorded at 22°C at 2-second intervals with an exposure time of 50 mseconds. Confocal images were acquired using a LEICA TCS SP2 microscope.

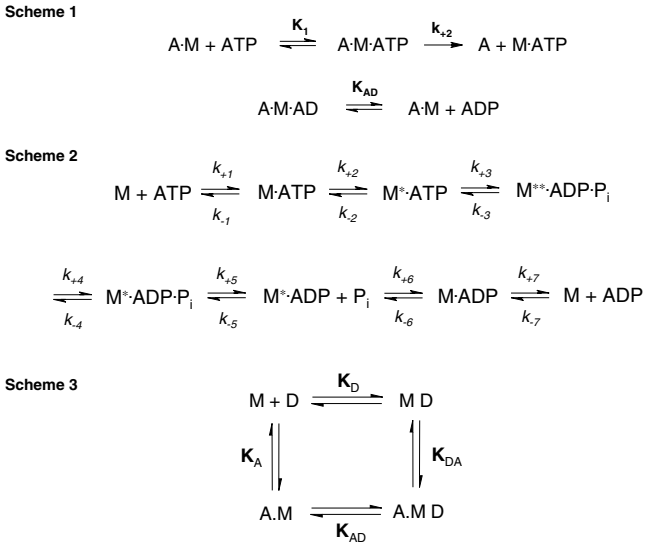

Fig. 6. The dynamics of ATP binding and hydrolysis by the myosin constructs were analyzed in terms of the models shown in Schemes 1-3, where M refers to myosin head fragment, A to actin, and T, D and P_i to ATP, ADP and phosphate, respectively. In these schemes, a notation is used that distinguishes between the constants in the presence and absence of actin by using bold ($\mathbf{K_{+1}}$, $\mathbf{K_1}$) versus italic type (k_{+1}, K_1); subscript A and D refer to actin ($\mathbf{K}_A$) and ADP (K_D), respectively.

We thank R. Schumann and S. Zimmermann for excellent technical assistance, E. D. Korn and H. Brzeska for providing myosin-I heavy chain kinase; M. Maniak for mAb176-2-5; R. Fedorov, and K. C. Holmes for helpful comments. The work was supported by grants Ma1081/5-3, Ma1081/6-1 (D.J.M.) and Ku1288/2-2 (F.J.K.).

References

Albanesi, J. P., Hammer, J. A., III and Korn, E. D. (1983). The interaction of F-actin with phosphorylated and unphosphorylated myosins IA and IB from *Acanthamoeba castellanii*. *J. Biol. Chem.* **258**, 10176-10181.

Anson, M., Geeves, M. A., Kurzawa, S. E. and Manstein, D. J. (1996). Myosin motors with artificial lever arms. *EMBO J.* **15**, 6069-6074.

Bagshaw, C. R., Eccleston, J. F., Eckstein, F., Goody, R. S., Gutfreund, H. and Trentham, D. R. (1974). The magnesium ion-dependent adenosine triphosphatase of myosin. Two-step processes of adenosine triphosphate association and adenosine diphosphate dissociation. *Biochem. J.* **141**, 351-364.

Bain, G. and Tsang, A. (1991). Disruption of the gene encoding the p34/31 polypeptides affects growth and development of *Dictyostelium discoideum*. *Mol. Gen. Genet.* **226**, 59-64.

Batra, R. and Manstein, D. J. (1999). Functional characterisation of *Dictyostelium* myosin II with conserved tryptophanyl residue 501 mutated to tyrosine. *Biol. Chem.* **380**, 1017-1023.

Batra, R., Geeves, M. A. and Manstein, D. J. (1999). Kinetic analysis of *Dictyostelium discoideum* myosin motor domains with glycine-to-alanine mutations in the reactive thiol region. *Biochemistry* **38**, 6126-6134.

Bement, W. M. and Mooseker, M. S. (1995). TEDS rule: a molecular rationale for

differential regulation of myosins by phosphorylation of the heavy chain head. *Cell Motil. Cytoskeleton* **31**, 87-92.
Berg, J. S., Powell, B. C. and Cheney, R. E. (2001). A millennial myosin census. *Mol. Biol. Cell* **12**, 780-794.
Bretschneider, T., Jonkman, J., Kohler, J., Medalia, O., Barisic, K., Weber, I., Stelzer, E. H., Baumeister, W. and Gerisch, G. (2002). Dynamic organization of the actin system in the motile cells of *Dictyostelium*. *J. Muscle Res. Cell Motil.* **23**, 639-649.
Brzeska, H. and Korn, E. D. (1996). Regulation of class I and class II myosins by heavy chain phosphorylation. *J. Biol. Chem.* **271**, 16983-16986.
Brzeska, H., Lynch, T. J., Martin, B. and Korn, E. D. (1989). The localization and sequence of the phosphorylation sites of *Acanthamoeba* myosins I. An improved method for locating the phosphorylated amino acid. *J. Biol. Chem.* **264**, 19340-19348.
Brzeska, H., Young, R., Knaus, U. and Korn, E. D. (1999). Myosin I heavy chain kinase: cloning of the full-length gene and acidic lipid-dependent activation by Rac and Cdc42. *Proc. Natl. Acad. Sci. USA* **96**, 394-399.
Coates, J. H., Criddle, A. H. and Geeves, M. A. (1985). Pressure-relaxation studies of pyrene-labelled actin and myosin subfragment 1 from rabbit skeletal muscle. Evidence for two states of acto-subfragment 1. *Biochem. J.* **232**, 351-356.
Coluccio, L. M. and Geeves, M. A. (1999). Transient kinetic analysis of the 130-kDa myosin I (MYR-1 gene product) from rat liver. A myosin I designed for maintenance of tension? *J. Biol. Chem.* **274**, 21575-21580.
Cremo, C. R. and Geeves, M. A. (1998). Interaction of actin and ADP with the head domain of smooth muscle myosin: implications for strain-dependent ADP release in smooth muscle. *Biochemistry* **37**, 1969-1978.
de Hostos, E. L., Bradtke, B., Lottspeich, F., Guggenheim, R. and Gerisch, G. (1991). Coronin, an actin binding protein of *Dictyostelium discoideum* localized to cell surface projections, has sequence similarities to G protein beta subunits. *EMBO J.* **10**, 4097-4104.
De La Cruz, E. M., Wells, A. L., Rosenfeld, S. S., Ostap, E. M. and Sweeney, H. L. (1999). The kinetic mechanism of myosin V. *Proc. Natl. Acad. Sci. USA* **96**, 13726-13731.
Egelhoff, T. T., Titus, M. A., Manstein, D. J., Ruppel, K. M. and Spudich, J. A. (1991). Molecular genetic tools for study of the cytoskeleton in *Dictyostelium*. *Meth. Enzymol.* **196**, 319-334.
El Mezgueldi, M., Tang, N., Rosenfeld, S. S. and Ostap, E. M. (2002). The kinetic mechanism of Myo1e (human myosin-IC). *J. Biol. Chem.* **277**, 21514-21521.
Epel, D. (2003). Protection of DNA during early development: adaptations and evolutionary consequences. *Evol. Dev.* **5**, 83-88.
Fujita-Becker, S., Dürrwang, U., Erent, M., Clark, R. J., Geeves, M. A. and Manstein, D. J. (2005). Changes in Mg^{2+} ion concentration and heavy chain phosphorylation regulate the motor activity of a class I myosin. *J. Biol. Chem.* **280**, 6064-6071.
Fukui, Y., Engler, S., Inoue, S. and de Hostos, E. L. (1999). Architectural dynamics and gene replacement of coronin suggest its role in cytokinesis. *Cell Motil. Cytoskeleton* **42**, 204-217.
Furch, M., Geeves, M. A. and Manstein, D. J. (1998). Modulation of actin affinity and actomyosin adenosine triphosphatase by charge changes in the myosin motor domain. *Biochemistry* **37**, 6317-6326.
Furch, M., Fujita-Becker, S., Geeves, M. A., Holmes, K. C. and Manstein, D. J. (1999). Role of the salt-bridge between switch-1 and switch-2 of *Dictyostelium* myosin. *J. Mol. Biol.* **290**, 797-809.
Geeves, M. A., Perreault-Micale, C. and Coluccio, L. M. (2000). Kinetic analyses of a truncated mammalian myosin I suggest a novel isomerization event preceding nucleotide binding. *J. Biol. Chem.* **275**, 21624-21630.
Gillespie, P. G., Albanesi, J. P., Bähler, M., Bement, W. M., Berg, J. S., Burgess, D. R., Burnside, B., Cheney, R. E., Corey, D. P., Coudrier, E. et al. (2001). Myosin-I nomenclature. *J. Cell Biol.* **155**, 703-704.
Gliksman, N. R., Santoyo, G., Novak, K. D. and Titus, M. A. (2001). Myosin I phosphorylation is increased by chemotactic stimulation. *J. Biol. Chem.* **276**, 5235-5239.
Hammer, J. A., III, Albanesi, J. P. and Korn, E. D. (1983). Purification and characterization of a myosin I heavy chain kinase from *Acanthamoeba castellanii*. *J. Biol. Chem.* **258**, 10168-10175.
Hiratsuka, T. (1983). New ribose-modified fluorescent analogs of adenine and guanine nucleotides available as substrates for various enzymes. *Biochim. Biophys. Acta* **742**, 496-508.
Ito, K., Kashiyama, T., Shimada, K., Yamaguchi, A., Awata, J., Hachikubo, Y., Manstein, D. J. and Yamamoto, K. (2003). Recombinant motor domain constructs of *Chara corallina* myosin display fast motility and high ATPase activity. *Biochem. Biophys. Res. Commun.* **312**, 958-964.
Jontes, J. D. and Milligan, R. A. (1997). Brush border myosin-I structure and ADP-dependent conformational changes revealed by cryoelectron microscopy and image analysis. *J. Cell Biol.* **139**, 683-693.
Jontes, J. D., Wilson-Kubalek, E. M. and Milligan, R. A. (1995). A 32 degree tail swing in brush border myosin I on ADP release. *Nature* **378**, 751-753.
Jung, G., Wu, X. and Hammer, J. A., III (1996). *Dictyostelium* mutants lacking multiple classic myosin I isoforms reveal combinations of shared and distinct functions. *J. Cell Biol.* **133**, 305-323.
Knetsch, M. L., Tsiavaliaris, G., Zimmermann, S., Ruhl, U. and Manstein, D. J. (2002). Expression vectors for studying cytoskeletal proteins in *Dictyostelium discoideum*. *J. Mus. Res. Cell Motil.* **23**, 605-611.
Kollmar, M., Dürrwang, U., Kliche, W., Manstein, D. J. and Kull, F. J. (2002). Crystal structure of the motor domain of a class-I myosin. *EMBO J.* **21**, 2517-2525.
Kron, S. J. and Spudich, J. A. (1986). Fluorescent actin filaments move on myosin fixed to a glass surface. *Proc. Natl. Acad. Sci. USA* **83**, 6272-6276.
Kurzawa, S. E. and Geeves, M. A. (1996). A novel stopped-flow method for measuring the affinity of actin for myosin head fragments using microgram quantities of protein. *J. Mus. Res. Cell Motil.* **17**, 669-676.
Kurzawa, S. E., Manstein, D. J. and Geeves, M. A. (1997). *Dictyostelium discoideum* myosin II: characterization of functional myosin motor fragments. *Biochemistry* **36**, 317-323.
Lee, S. F. and Cote, G. P. (1995). Purification and characterization of a *Dictyostelium* protein kinase required for actin activation of the Mg^{2+} ATPase activity of *Dictyostelium* myosin ID. *J. Biol. Chem.* **270**, 11776-11782.
Lee, S. F., Egelhoff, T. T., Mahasneh, A. and Cote, G. P. (1996). Cloning and characterization of a *Dictyostelium* myosin I heavy chain kinase activated by Cdc42 and Rac. *J. Biol. Chem.* **271**, 27044-27048.
Maniak, M. (2001). Fluid-phase uptake and transit in axenic *Dictyostelium* cells. *Biochim. Biophys. Acta* **1525**, 197-204.
Maniak, M., Rauchenberger, R., Albrecht, R., Murphy, J. and Gerisch, G. (1995). Coronin involved in phagocytosis: dynamics of particle-induced relocalization visualized by a green fluorescent protein Tag. *Cell* **83**, 915-924.
Manstein, D. J. and Hunt, D. M. (1995). Overexpression of myosin motor domains in *Dictyostelium*: screening of transformants and purification of the affinity tagged protein. *J. Mus. Res. Cell Motil.* **16**, 325-332.
Manstein, D. J., Ruppel, K. M. and Spudich, J. A. (1989). Expression and characterization of a functional myosin head fragment in *Dictyostelium discoideum*. *Science* **246**, 656-658.
Manstein, D. J., Schuster, H. P., Morandini, P. and Hunt, D. M. (1995). Cloning vectors for the production of proteins in *Dictyostelium discoideum*. *Gene* **162**, 129-134.
Michailova, A. and McCulloch, A. (2001). Model study of ATP and ADP buffering, transport of Ca^{2+} and Mg^{2+}, and regulation of ion pumps in ventricular myocyte. *Biophys. J.* **81**, 614-629.
Millar, N. C. and Geeves, M. A. (1983). The limiting rate of the ATP-mediated dissociation of actin from rabbit skeletal muscle myosin subfragment 1. *FEBS Lett.* **160**, 141-148.
Novak, K. D. and Titus, M. A. (1997). Myosin I overexpression impairs cell migration. *J. Cell Biol.* **136**, 633-647.
Novak, K. D. and Titus, M. A. (1998). The myosin I SH3 domain and TEDS rule phosphorylation site are required for in vivo function. *Mol. Biol. Cell* **9**, 75-88.
Novak, K. D., Peterson, M. D., Reedy, M. C. and Titus, M. A. (1995). *Dictyostelium* myosin I double mutants exhibit conditional defects in pinocytosis. *J. Cell Biol.* **131**, 1205-1221.
Nyitrai, M. and Geeves, M. A. (2004). Adenosine diphosphate and strain sensitivity in myosin motors. *Philos. Trans. R. Soc. Lond. B Biol. Sci.* **359**, 1867-1877.
Ostap, E. M., Lin, T., Rosenfeld, S. S. and Tang, N. (2002). Mechanism of regulation of *Acanthamoeba* myosin-IC by heavy-chain phosphorylation. *Biochemistry* **41**, 12450-12456.
Rosenfeld, S. S., Houdusse, A. and Sweeney, H. L. (2005). Magnesium regulates ADP dissociation from myosin V. *J. Biol. Chem.* **280**, 6072-6079.
Ruff, C., Furch, M., Brenner, B., Manstein, D. J. and Meyhofer, E. (2001). Single-molecule tracking of myosins with genetically engineered amplifier domains. *Nat. Struct. Biol.* **8**, 226-229.
Satre, M. and Martin, J. B. (1985). ^{31}P-nuclear magnetic resonance analysis of the intracellular pH in the slime mold *Dictyostelium discoideum*. *Biochem. Biophys. Res. Commun.* **132**, 140-146.
Siemankowski, R. F. and White, H. D. (1984). Kinetics of the interaction between actin, ADP, and cardiac myosin-S1. *J. Biol. Chem.* **259**, 5045-5053.
Spudich, J. A. and Watt, S. (1971). The regulation of rabbit skeletal muscle contraction. I. Biochemical studies of the interaction of the tropomyosin-troponin complex with actin and the proteolytic fragments of myosin. *J. Biol. Chem.* **246**, 4866-4871.
Titus, M. A., Wessels, D., Spudich, J. A. and Soll, D. (1993). The unconventional myosin encoded by the MyoA gene plays a role in *Dictyostelium* motility. *Mol. Biol. Cell* **4**, 233-246.
Toyoshima, Y. Y., Kron, S. J., McNally, E. M., Niebling, K. R., Toyoshima, C. and Spudich, J. A. (1987). Myosin subfragment-1 is sufficient to move actin filaments in vitro. *Nature* **328**, 536-539.
Tsiavaliaris, G., Fujita-Becker, S. and Manstein, D. J. (2004). Molecular engineering of a backwards-moving myosin motor. *Nature* **427**, 558-561.
Urrutia, R. A., Jung, G. and Hammer, J. A., III (1993). The *Dictyostelium* myosin IE heavy chain gene encodes a truncated isoform that lacks sequences corresponding to the actin binding site in the tail. *Biochim. Biophys. Acta* **1173**, 225-229.
Veigel, C., Coluccio, L. M., Jontes, J. D., Sparrow, J. C., Milligan, R. A. and Molloy, J. E. (1999). The motor protein myosin-I produces its working stroke in two steps. *Nature* **398**, 530-533.
Wienke, D. C., Knetsch, M. L., Neuhaus, E. M., Reedy, M. C. and Manstein, D. J. (1999). Disruption of a dynamin homologue affects endocytosis, organelle morphology, and cytokinesis in *Dictyostelium discoideum*. *Mol. Biol. Cell* **10**, 225-243.
Woodward, S. K., Eccleston, J. F. and Geeves, M. A. (1991). Kinetics of the interaction of 2′(3′)-O-(N-methylanthraniloyl)-ATP with myosin subfragment 1 and actomyosin subfragment 1, characterization of two acto-S1-ADP complexes. *Biochemistry* **30**, 422-430.
Yamashita, R. A. and May, G. S. (1998). Constitutive activation of endocytosis by mutation of myoA, the myosin I gene of *Aspergillus nidulans*. *J. Biol. Chem.* **273**, 14644-14648.